Thermally Annealed Anisotropic Graphene Aerogels and Their Electrically Conductive Epoxy Composites with Excellent Electromagnetic Interference Shielding Efficiencies

Li, Xing-Hua; Li, Xiaofeng; Liao, Kai-Ning; Min, Peng; Liu, Tao; Dasari, Aravind; Yu, Zhong-Zhen

2016

Li, X.-H., Li, X., Liao, K.-N., Min, P., Liu, T., Dasari, A., et al. (2016). Thermally Annealed Anisotropic Graphene Aerogels and Their Electrically Conductive Epoxy Composites with Excellent Electromagnetic Interference Shielding Efficiencies. ACS Applied Materials & Interfaces, 8(48), 33230-33239.

https://hdl.handle.net/10356/85721

https://doi.org/10.1021/acsami.6b12295

Thermally Annealed Anisotropic Graphene Aerogels and Their Electrically Conductive Epoxy Composites with Excellent Electromagnetic Interference Shielding Efficiencies

Xing-Hua Li[a], *Xiaofeng Li*[a*], *Kai-Ning Liao*[a], *Peng Min*[a], *Tao Liu*[a], *Aravind Dasari*[b] *and Zhong-Zhen Yu*[a,c*]

[a] State Key Laboratory of Organic-Inorganic Composites, College of Materials Science and Engineering, Beijing University of Chemical Technology, Beijing 100029, China

[b] School of Materials Science & Engineering (Blk N4.1), Nanyang Technological University, 50 Nanyang Avenue, Singapore 639798

[c] Beijing Advanced Innovation Center for Soft Matter Science and Engineering, Beijing University of Chemical Technology, Beijing 100029, China

ABSTRACT: Mechanical and functional properties of polymer/graphene nanocomposites are affected by dispersion and spatial distribution of graphene sheets in the polymer matrix. Anisotropic graphene aerogels (AGAs) with highly aligned graphene networks are prepared by a directional-freezing followed by freeze-drying process and exhibit different microstructures and performances along the axial (freezing direction) and radial (perpendicular to the axial direction) directions. Thermal annealing at 1300 ^{o}C significantly enhances the quality of both AGAs and conventional graphene aerogels (GAs). The aligned

graphene/epoxy composites show highly anisotropic mechanical and electrical properties and excellent electromagnetic interference (EMI) shielding effectiveness at very low graphene loadings. Compared to the epoxy composite with 0.8 wt% thermally annealed GAs (TGAs) with an EMI shielding effectiveness of 27 dB, the aligned graphene/epoxy composite with 0.8 wt% thermally treated AGAs (TAGAs) has an enhanced EMI shielding effectiveness of 32 dB in the radial direction with a slightly decreased shielding effectiveness of 25 dB in the axial direction. With 0.2 wt% of TAGA, its epoxy composite exhibits a shielding effectiveness of 25 dB in the radial direction, which meets the shielding effectiveness requirement of 20 dB for practical EMI shielding applications. To our best knowledge, this is the lowest filler content for all graphene based composites with the similar EMI shielding performance.

KEYWORDS: anisotropic graphene aerogel; electromagnetic interference shielding; electrical conductivity; directional freezing; epoxy

1. Introduction

The electromagnetic pollution in the past decade has resulted in rapid developments of electrically conductive carbon/polymer nanocomposites for electromagnetic interference (EMI) shielding and absorption.[1-3] Among various carbon materials[4-7], graphene has stimulated extensive interests due to its remarkable specific surface area,[6,7] mechanical properties,[8] thermal conductivity[9] and electrical conductivity.[10] A variety of conductive graphene/polymer nanocomposites with high EMI shielding performances have been developed by dispersing graphene sheets into polymer matrices. It has been well reported

that dispersion and spatial distribution of graphene sheets in the polymer matrix are crucial for endowing polymers with high electrical conductivity and EMI shielding effectiveness (SE).[11-13] As the enhanced electrical and EMI shielding performances are usually obtained at the expense of ductility and toughness of the conductive polymer nanocomposites,[12-14] For this purpose, many have emphasized on designing and fabricating three-dimensional (3D) polymer nanocomposite aerogels and foams by forming a special structure[15] or using preformed.[16-18] The formation of graphene aerogels and foams not only avoids the restacking of individual graphene sheets, but also endows a porous and less dense 3D architecture. This architecture is more efficient in constructing an electrically conducting network even at lower loadings than powdery fillers.[17,19-22] Furthermore, the numerous cell/wall interfaces in the 3D architecture also benefit the attenuation of incident electromagnetic waves by enhancing the multi-reflection of the incident waves.[19-22]

Graphene aerogels and foams are fabricated by self-assembly,[23-28] template-assisted assembly[29,30] and chemical vapor deposition (CVD),[31] and their polymer composites can be readily prepared by infiltration of polymers or monomers into the 3D graphene networks. For example, Cheng et al.[18] fabricated a lightweight and highly conductive graphene /polydimethylsiloxane (PDMS) foam by infiltration of PDMS into graphene foam that was prepared by CVD approach. The foam composite exhibited a high EMI shielding effectiveness of more than 30 dB at a relatively low graphene loading of 0.8 wt.%. Comparatively, traditional polymer composite even with 15 wt.% of graphene show an EMI SE of 21 dB only in the X-band.[32]

Another advancement in this field is the preparation of graphene aerogels with anisotropic microstructure. The alignment of carbon fillers in a polymer matrix along the direction perpendicular to the incidental waves will benifit the efficient utilization of the carbon/polymer interfaces to enhance multi-reflection and thus attenuation of the incident waves. This anisotropy, for example, is accomplished by directional-freezing of graphene hydrogels followed by freezee-drying.[33] Zhang et al.[13] prepared anisotropic multiwalled carbon nanotube/water-borne polyurethane (MWCNT/WPU) porous composites. The aligned porous sturcture enhanced the EMI shieding in the specific direciton (50 dB with 7.2 vol% of MWCNTs). An epoxy thin film with aligned graphene sheets also exhibited an excellent EMI SE of 38 dB at a low loading of 2 wt%.[34] However, till now, nothing much has been reported on studying the EMI shielding performance of polymer composites with AGAs as the electrically conductive network, and how the anisotropic structure improves the EMI shielding performances deserves further investigation.

In this work, we demonstrate a template-free approach to prepare highly anisotropic AGAs by self-assembly of chemically reduced GO, directional-freezing, and freeze-drying processes.[35] To further enhance their conductivities, AGAs are thermally annealed at 1300 ^{o}C in an inert atmosphere to remove the residual oxygen-containing groups and defects.[36] Further, the anisotropic porous architecture is retained even after impregnating with epoxy monomer and curing agents. Due to the aligned graphene network and the high temperature annealing, the epoxy composites show significantly improved both electrical and EMI shielding performances.

2. Experimental

2.1 Materials

Concentrated sulfuric acid (H_2SO_4, 98%), nitric acid (HNO_3, 70%), sodium nitrate ($NaNO_3$), potassium permanganate ($KMnO_4$), hydrogen peroxide (H_2O_2, 38%), hydrochloric acid (HCl, 38%), ethanol, and ascorbic acid were purchased from Beijing Chemical Factory (China). Pristine graphite was supplied by Huadong Graphite Factory (China). Epoxy resin (JY-257) with an epoxy value of 0.53-0.55 mol/100g was obtained from Jiafa Chemical Co. (China). Methyl hexahydrophthalic anhydride as the curing agent and tris-(dimethyl aminomethyl) phenol as the curing accelerator were purchased from Alfa Aesar (China).

2.2 Preparation of AGAs and GAs and their thermal annealing

Graphite oxide was prepared according to the modified Hummers method.[37] GO aqueous suspensions (2-10 mg/ml) were prepared by sonicating the mixer of graphite oxide and deionized water in an 80 ml beaker. After ascorbic acid was added as a mild reduction agent,[38,39] the suspension of GO and ascorbic acid (1/1, w/w) was mixed by ultrasonication using a JY92-IIDN ultrasonicator (China) at 270 W for 10 min, and heated in an oven at 65 ^{o}C for 3 h and 75 ^{o}C for 1 h to obtain graphene hydrogel. After cooling to room temperature, the graphene hydrogel was dialyzed in deionized water to remove soluble species, and then subjected to two different approaches: (1) directional freezing by placing the hydrogel on a Cu disk that was floating on liquid nitrogen.[40] The hydrogel was vertically frozen from its bottom surface in contact with Cu disk to the top surface, and the resulting anisotropic graphene hydrogel was then freeze-dried in a FD-1C-50 freeze drier to

obtain a 3D AGA. (2) For comparison, conventional graphene aerogel (GA) was also prepared by freezing the graphene hydrogel at -18 °C in a normal refrigerator followed by freeze-drying in the freeze drier. The preparation processes of GA and AGA are schematically illustrated in Figure 1. To improve their quality, AGA and GA were thermally annealed at 1300 °C for 2 h in a flowing argon atmosphere in an OTF-1200X-100-II tube furnace (China) and the thermally annealed AGA and GA aerogels were designated as TAGA and TGA, respectively.

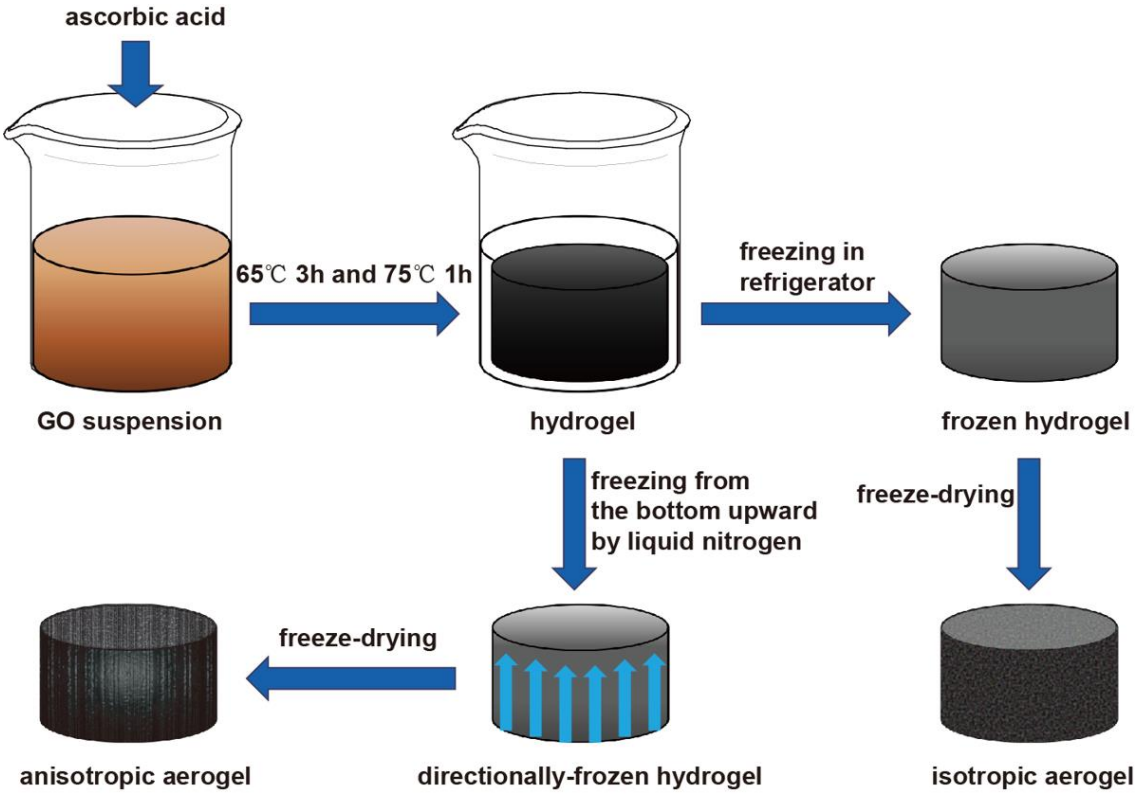

Figure 1. A schematic illustrating the fabrication procedure of GA and AGA.

2.3 Preparation of AGA/epoxy and TAGA/epoxy composites

The epoxy resin, the curing agent and the accelerator with a weight ratio of 100/89/1 were mechanically mixed in a beaker. AGA or TAGA was immersed and backfilled by the mixture in a vacuum oven for 30 min, cured at 80 °C for 4 h followed by 120 °C for 2 h to

prepare AGA/epoxy and TAGA/epoxy composites for the measurements of EMI shielding and mechanical properties.

2.4 EMI shielding measurements

Parameters of S_{11} and S_{21} for the epoxy composites were measured on a Wiltron 54169A scalar measurement system using the wave guide method in the X-band frequency of 8-12 GHz. S_{11} represents measured reflection coefficient data, and S_{21} represents transmission data. As the values of measured S_{11} and S_{21} are negative, the values of $|S_{11}|$ and $|S_{21}|$ are called the attenuations on reflection and transmission of the incident waves, respectively. The power coefficients reflectivity (R), transmissivity (T) and absorptivity (A) were calculated according to the following equations.[19,21,41,42]

$$R = 10^{(S_{11}/10)} \quad (1)$$

$$T = 10^{(S_{21}/10)} \quad (2)$$

$$A = 1 - R - T \quad (3)$$

The total EMI SE (SE_{Total}) of a composite consists of the contributions from reflection (SE_R), absorption (SE_A) and multiple reflections (SE_M), and their relationship is that:

$$SE_{Total} = SE_R + SE_A + SE_M \quad (4)$$

When $SE_{Total} > 15$ dB, it is usually assumed that:

$$SE_{Total} \approx SE_R + SE_A \quad (5)$$

The EMI SE due to reflectance and effective absorbance can be described by Eq.s 6 and 7.[19,21,41-43]

$$SE_R = -10 \log (1-R) \quad (6)$$

$$SE_A = -10 \log (T/ (1-R)) \quad (7)$$

2.5 Characterization

X-ray diffraction (XRD) patterns of GO, AGA and TAGA were recorded with a Rigaku D/Max 2500 X-ray diffractometer using CuKα radiation (λ= 1.54 Å) at a generator current of 50 mA and a generator voltage of 40 kV with a scanning speed of 4^{o}/min. The chemical compositions of GA, AGA, TGA and TAGA were analyzed with a ThermoFisher Escalab 250 X-ray photoelectron spectroscopy (XPS). GA, AGA, TGA and TAGA were also scanned with a 65 Renishaw in Via Raman microscopy to evaluate their qualities. Microstructures of GA, AGA and their epoxy composites were observed with a ZEISS Supra 55 scanning electron microscope (SEM) and a Nikon ECLIPSE Ci-POL microscope (Japan). Electrical conductivities of the epoxy composites were measured with a 4-probes-Tech RTS-8 resistivity meter (China). Storage modulus curves were recorded by a Rheometric Scientific Model-V dynamic mechanical analyzer (DMA) using a single-cantilever mode from 25 to 180 ^{o}C with a heating speed of 5 ^{o}C/min at 1 Hz. For the test along the axial direction, graphene sheets are aligned along the thickness direction of the specimens with dimensions of $30\times3\times1$ mm^3; While for the test along the radial direction, graphene sheets are aligned along the length direction of the specimens.

3. Results and discussion

3.1 Morphology and Chemical compositions of AGA and TAGA

Figures 2a-c show a typical foam structure of TAGA, revealing highly aligned pores along the freezing direction. In a typical directional freezing process, the water in the hydrogel is frozen from the bottom of the beaker and the ice grows along the freezing direction. The growing ice crystals exclude graphene sheets from the freezing front, leading to aligned

structures in the axial direction.[40] During the subsequent freeze drying process, ice sublimation leaves the aligned pores and thereby a monolithic AGA with anisotropic porous structure is obtained. More importantly, even after annealing the sample at 1300 ^{o}C, graphene sheets still maintained their aligned architecture (Figure 2c). However, TGA, which was prepared by freeze-drying of graphene hydrogel (frozen in refrigerator) followed by annealing at 1300 ^{o}C, exhibited an isotropic macroporous structure with distributed pores (Figure 2d). By varying the GO concentration, AGAs and GAs with different densities are obtained.

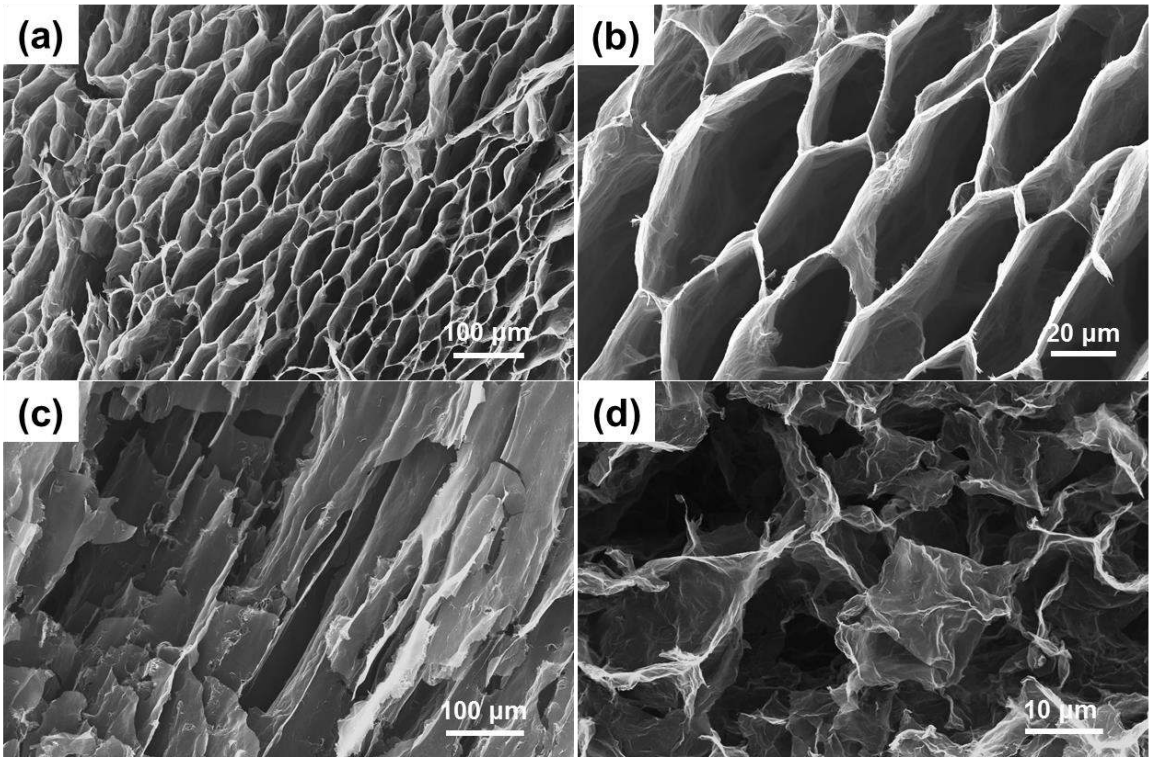

Figure 2. SEM images of the porous structures of (a,b) TAGA (top-view), (c) TAGA (side-view), and (d) TGA. The densities of TAGA and AGA are ~9.2 mg cm^{-3}.

Further, to confirm the complete oxidation of GO, XRD was carried out and the patterns of GO, AGA and TAGA are shown in Figure S1. GO does not present the characteristic peak of pristine graphite at 26.5^{o},[25] indicating the complete oxidation of graphite. Instead,

its new peak at 12° is ascribed to the enlarged intra-gallery by intercalation of oxygen-containing groups. Even AGA does not show such peaks in its XRD pattern, indicating the reduction and exfoliation of GO. However, when AGA is thermally reduced at 1300 °C, the diffraction pattern shows a small and broad peak at 26.5°, suggesting the restacking of the exfoliated graphene sheets

Figure 3 shows the XPS spectra of GO, AGA and TAGA. GO exhibits four types of carbon with different valences: C-C at ~284.5 eV, C-O at 286.6 eV, C=O at 287.8 eV, and O-C=O at 289.0 eV. Compared to GO, AGA exhibits a great reduction in the O 1s peak intensity, implying the removal of oxygen-containing groups of GO due to the chemical reduction by ascorbic acid during the synthesis of graphene hydrogel.[38] After the thermal annealing of AGA, the peaks of these oxygen-containing groups are further weakened in the XPS C 1s pattern of TAGA (Fig. 3c,d,S2b,S2c). The C/O atomic ratio of TAGA is up to 37.3, much higher than that of AGA (4.9) and GO (2.1), indicating the highly efficient reduction of AGA during the high temperature thermal annealing. The higher reduction extent of TAGA than AGA and GO results in a higher electrical conductivity for TAGA. For comparison, Figure S2b and S2c show the C 1s spectra of GA and TGA, which also confirm the significant reduction of GA by the thermal annealing.

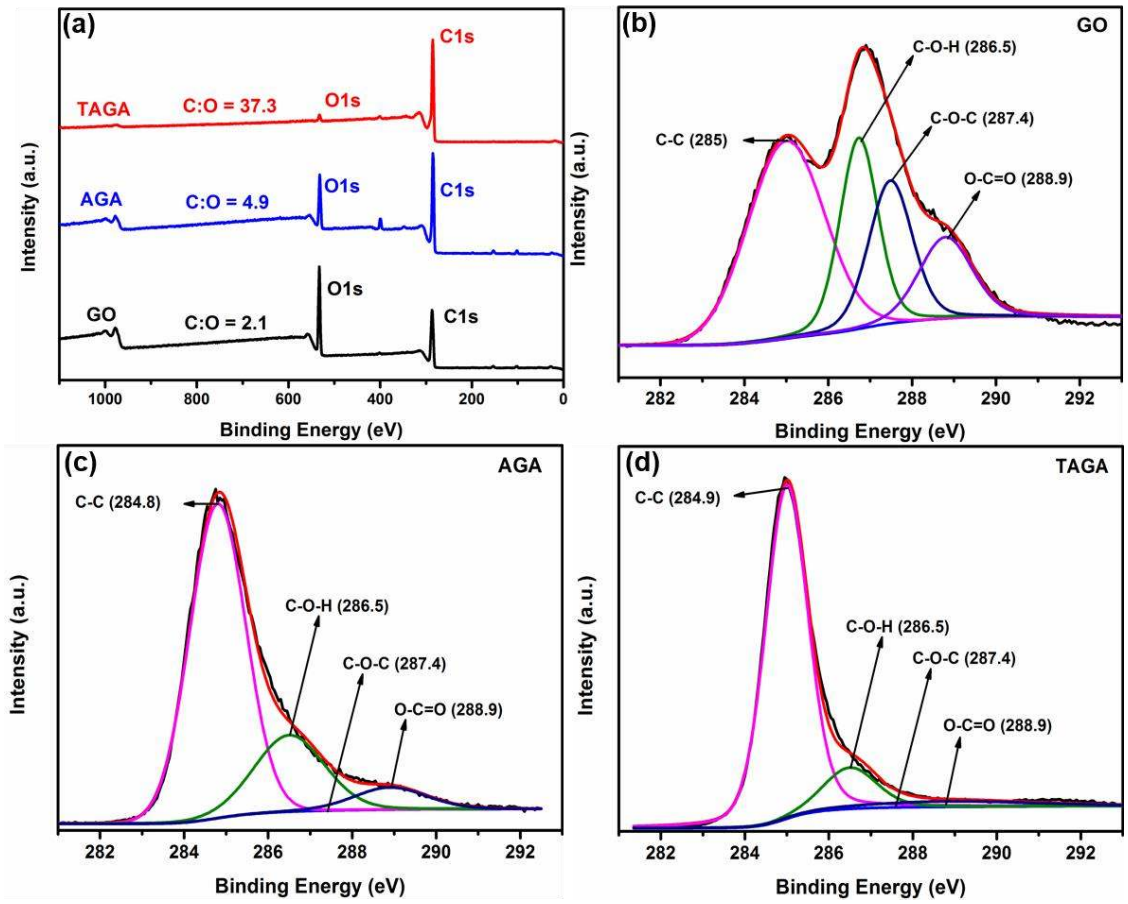

Figure 3. (a) XPS board scan spectra of GO, AGA and TAGA; XPS C1s curves of (b) GO, (c) AGA and (d) TAGA.

Figure 4 shows Raman spectra of GO, AGA and TAGA. GO presents two typical peaks of G band at 1601 cm^{-1} and D band at 1350 cm^{-1}. The D band is an indication of structural defects and disordered structure of graphitic domains, whereas the G band results from the in-plane stretching of the graphite lattice. For AGA, although the removal of oxygen-containing groups from GO sheets by the chemical reduction should re-establish the conjugated G network, the size of the network is believed to be smaller than the pristine one, consequently increasing the intensity ratio of D to G bands (I_D/I_G) from 0.93 of GO to 1.21 for AGA. However, the thermal annealing at 1300 ^oC is more efficient in the reduction of AGA and obviously decreases the D/G band intensity ratio to 0.89, indicating the

repairing of a considerable number of defects.[36,44] Besides, Raman spectra of GA and TGA (Fig. S3) are also similar to those of AGA and TAGA. By combining the XPS and Raman spectra results, it is confirmed that the GO component is well chemically reduced by ascorbic acid and thermally reduced at 1300 ^{o}C.[38]

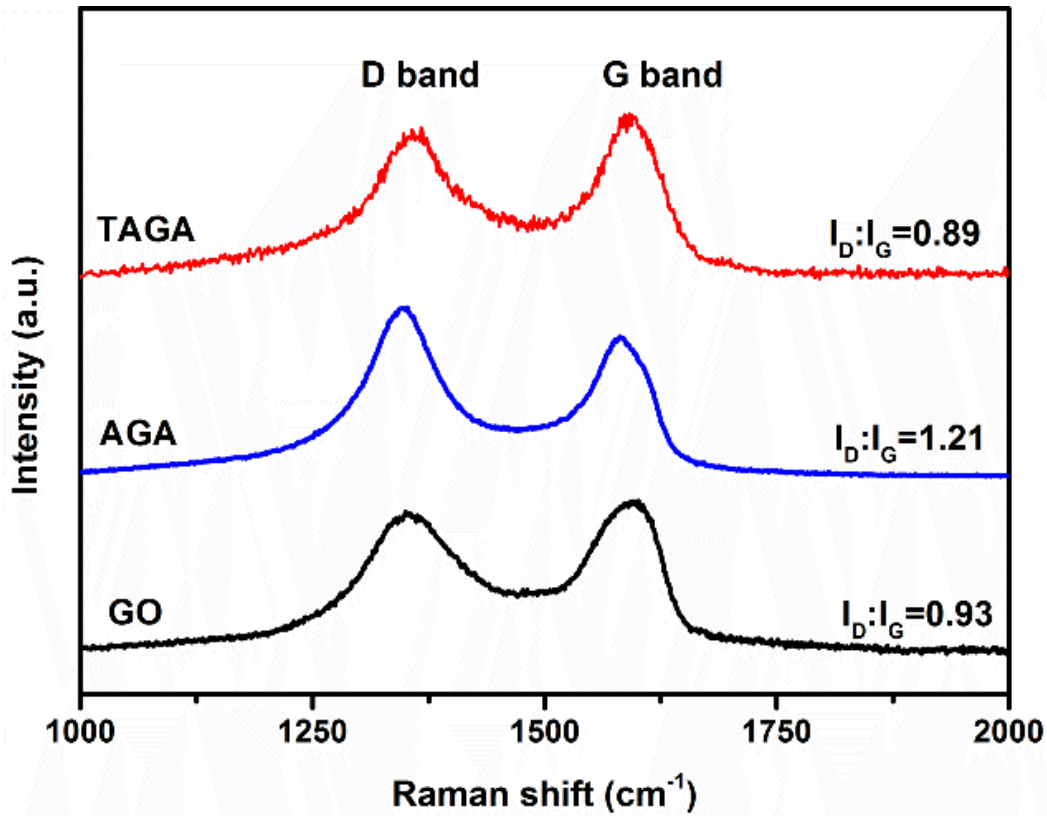

Figure 4. Raman spectra of GO, AGA and TAGA.

3.2 Microstructure and electrical properties of epoxy composites

Figure 5 shows SEM micrographs of freeze-fracture surfaces of epoxy composites with 0.8 wt% of graphene (epoxy/TAGA0.8 and epoxy/TGA0.8). The side-view of the epoxy/TAGA0.8 composite (Fig. 5a) clearly presents a highly anisotropic structure due to the aligned porous architecture, while its top-view SEM image (Fig. 5b) shows many irregular domains. The top-view optical micrograph (Fig. 5c) clearly exhibits a continuous

network composed by the cell walls of TAGA. Differently, the epoxy/TGA0.8 composite exhibits a homogeneous structure without anisotropic architecture (Fig. 5d).

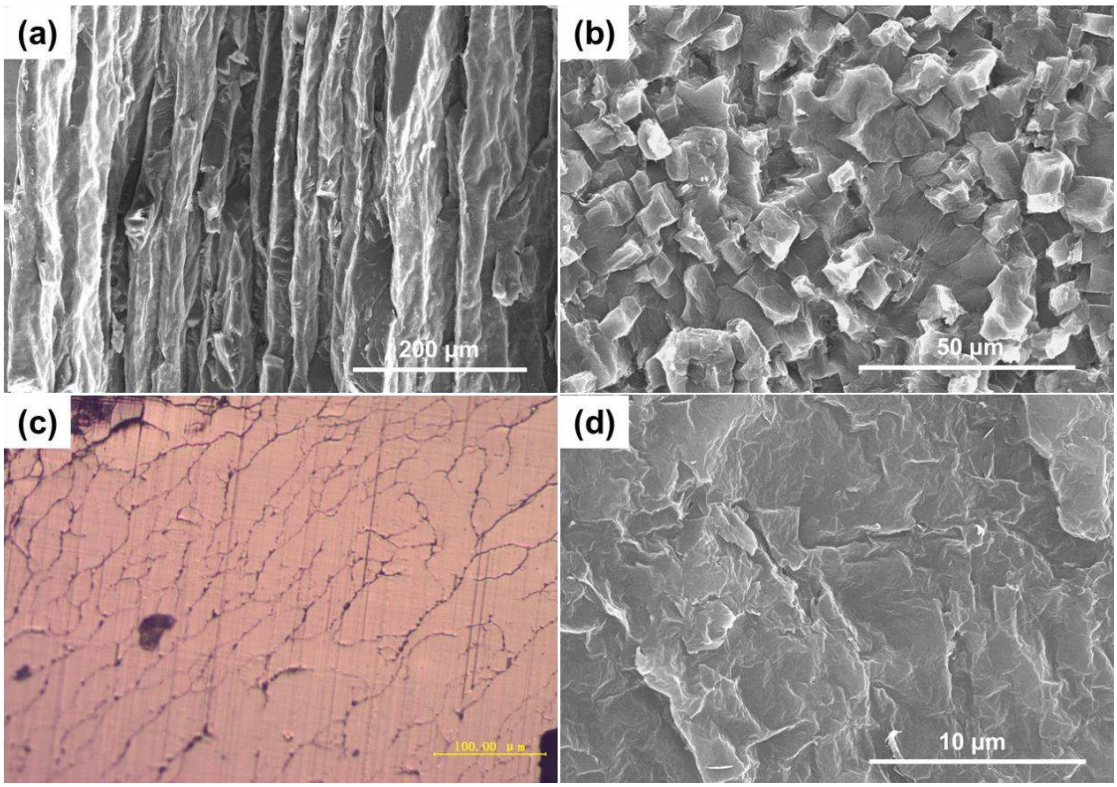

Figure 5. (a) Side-view and (b) top-view SEM images of freeze-fracture surfaces of epoxy/TAGA0.8 composite. (c) Top-view optical micrograph of a polished surface of epoxy/TAGA0.8 composite. (d) SEM image of freeze-fracture surface of epoxy/TGA0.8 composite.

The anisotropic architecture of TAGA results in different electrical and EMI shielding performances in axial and radial directions (Fig. 6). TAGA composites show substantially higher electrical conductivities than AGA composites due to the thermal reduction of AGA during the annealing process. Furthermore, TAGA composites exhibit different electrical conductivities in the radial and axial directions. For example, the electrical conductivity of the composite with 0.8 wt% TAGA is 980 S/m along axial direction but it is only 96 S/m along the radial direction, which is ascribed to the aligned stacking of graphene sheets

along the axial direction and thus a good conducting network with high electron mobility.[45] Even at a low TAGA loading of 0.2 wt%, the electrical conductivity reaches 26 S/m in the axial direction, indicating that such a low content of graphene sheets is sufficient to construct an conducting network in the matrix. The lower conductivity along the radial direction results from the gaps between the aligned graphene domains left after the sublimation of ice rods.

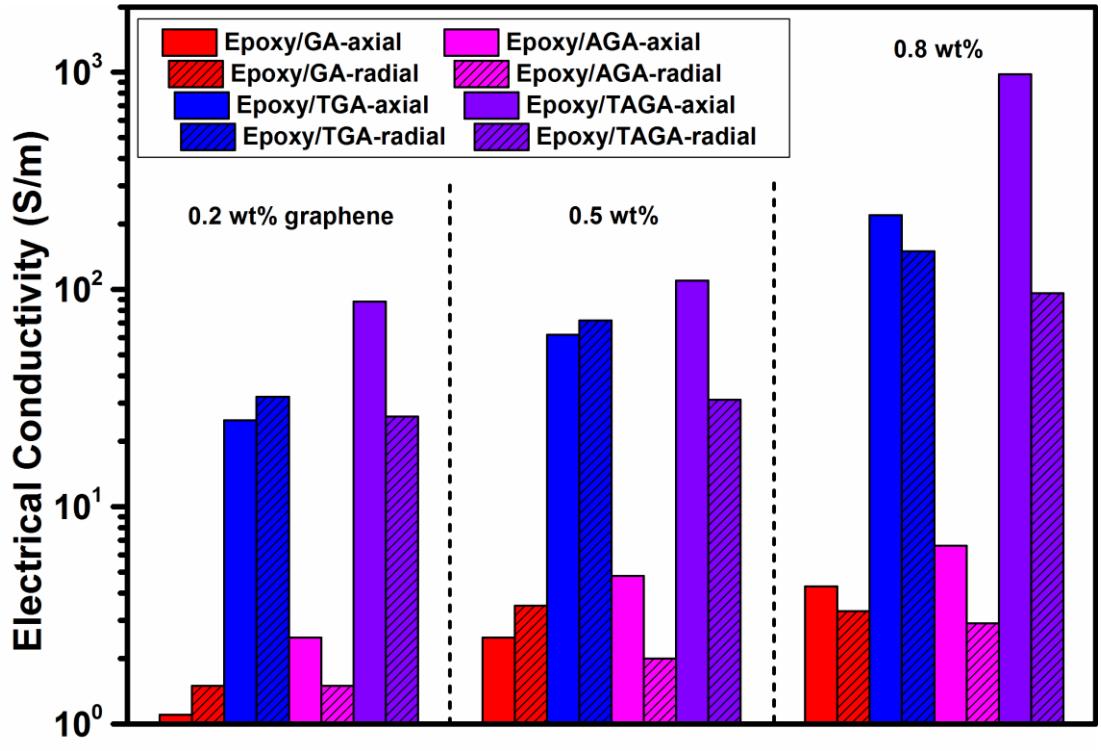

Figure 6. Electrical properties of composites with GA, TGA, AGA and TAGA in axial and radial directions.

3.3 EMI shielding performances of the epoxy composites along axial and radial directions

Inspired by the remarkable and highly anisotropic electrical conductivities, the EMI shielding properties of the epoxy/TAGA composites are measured in the frequency range of 8-12 GHz along both axial and radial directions (Fig. 7a-c). The alignment of the graphene sheets along the axial direction generates numerous polymer/graphene interfaces in the

radial direction, significantly benefiting multi-reflection and attenuation of the incident waves (Fig. 8).[13,46] As a result, the mean value of EMI SE for the epoxy composite with 0.8 wt% TAGA along the radial direction is 32 dB, much higher than that along the axial direction (25 dB), and also better than that of the composite with 0.8 wt% TGA (27 dB). However, if individual graphene sheets are filled in a polymer matrix, a much higher loading of 5 wt% or more would be required to achieve such an EMI shielding performance.[21] Even 0.2 wt% TAGA brings about an EMI SE of 25 dB along the radial direction, implying that more than 99% electromagnetic waves are shielded. To the best of our knowledge, this is comparable to the best EMI shielding performance reported for graphene based polymer composites (Table S1).[13,14,18,19,21,32,34,47,48]

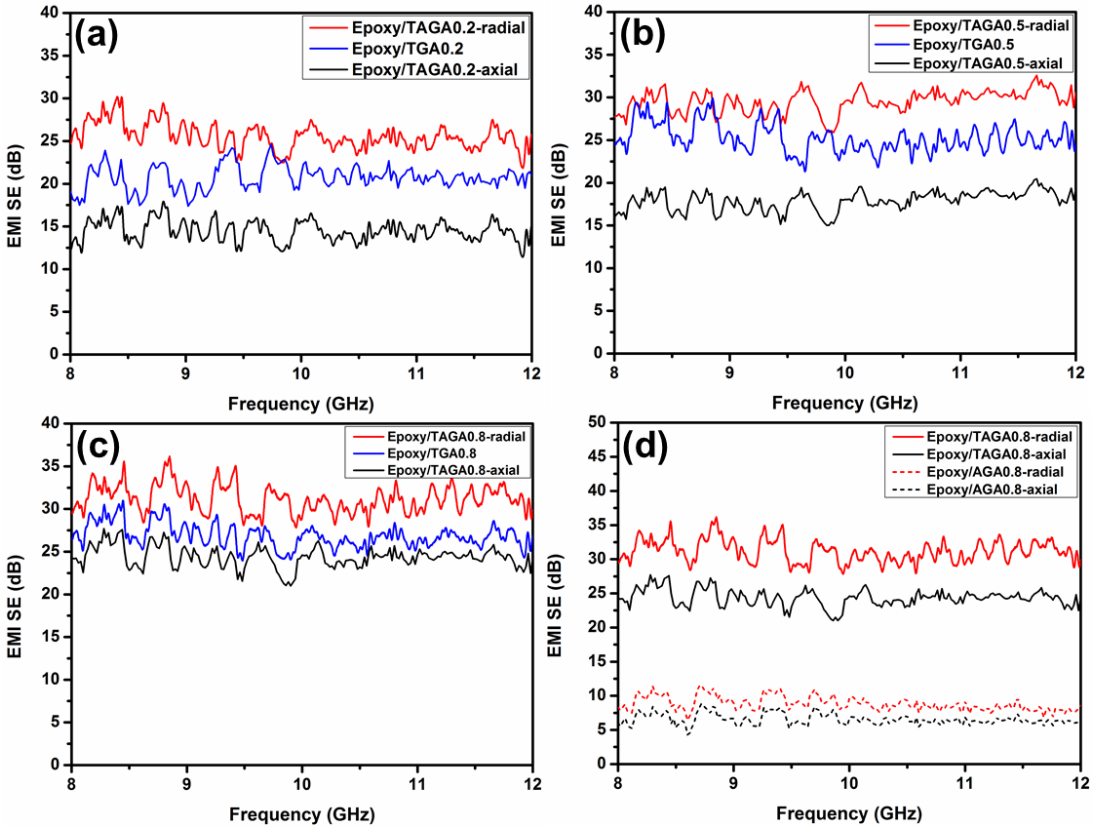

Figure 7. Plots of EMI SE versus frequency for epoxy composites with various TGA or TAGA contents of (a) 0.2 wt%, (b) 0.5 wt% and (c) 0.8 wt%. (d) Plots of EMI SE for

epoxy/AGA0.8 and epoxy/TAGA0.8 composites in axial and radial directions. The thickness of the specimens is kept at 4 mm unless otherwise stated.

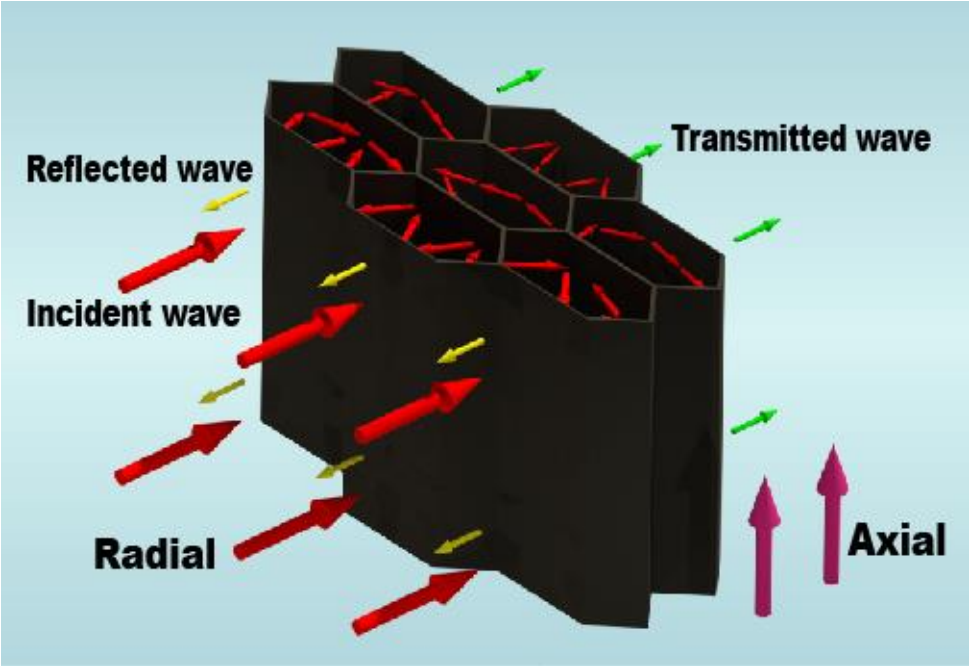

Figure 8. Schematic illustrating the EMI shielding mechanisms for anisotropic epoxy/graphene composites along radical and axial directions.

With increasing the TAGA content to 0.5 and 0.8 wt%, the electrical conductivity of the composite increases from 110 to 980 S/m along the axial direction and from 31 to 96 S/m along the radial direction. Their EMI SE values present a similar trend. The enhanced electrical conductivity benefits the improved EMI SE of the epoxy/TAGA composites.

The advantage of thermal annealing is well reflected by comparing the EMI shielding performances of the epoxy composites with 0.8 wt% TAGA or AGA (Fig. 7d). With 0.8 wt% of TAGA, the composite exhibits high EMI SE values of 32 and 25 dB along radial and axial directions, respectively. Whereas, its counterpart with 0.8 wt% AGA shows much lower EMI SE values of 8 and 6 dB along the radial and axial directions, respectively. Similar results are shown in Figure S4 for epoxy/GA0.8 and epoxy/TGA0.8 composites.

The comparisons of electrical conductivity (Fig. 6) and EMI SE (Fig. 7d) of epoxy/TAGA0.8 and epoxy/AGA0.8 composites confirm the superiority of the thermal annealing at 1300 ^{o}C. The higher EMI SE of the TAGA composites than that of the AGA counterparts is attributed to the further thermal reduction and significantly enhanced electrical conductivity.[49]

The EMI SE is not only dependent on the intrinsic electrical conductivity and dispersion quality of the fillers, but also on the volume and thickness of the composite samples.[50] By increasing the specimen thickness from 2 to 4 mm, the EMI SE average value of the epoxy/TAGA0.8 composite along the radial direction increases from 22 to 32 dB (Fig. 9a). Similarly, the average value of EMI SE along the axial direction increases from 15 to 25 dB (Fig. 9b). Similar results are observed for the epoxy/TGA0.8 composites with different thicknesses (Fig. S5). The electrically conductive graphene network provides interfaces to weaken the incident EM waves by multiple reflections and the increase in thickness enhances both the reflection and multiple reflection inside the composites.[51] To investigate the EMI shielding mechanisms along the two directions, the total EMI SE (SE_{Total}) and the contributions from absorption (SE_A) and reflection (SE_R) are compared (Fig. 9c).[13] It is clear that both SE_A and SE_R along the radical direction are higher than those along the axial direction because of the alignment of the graphene sheets. In addition, the much smaller SE_R in both directions than corresponding SE_A indicates that the contribution of absorption to the total EMI SE is much larger than that of reflection.

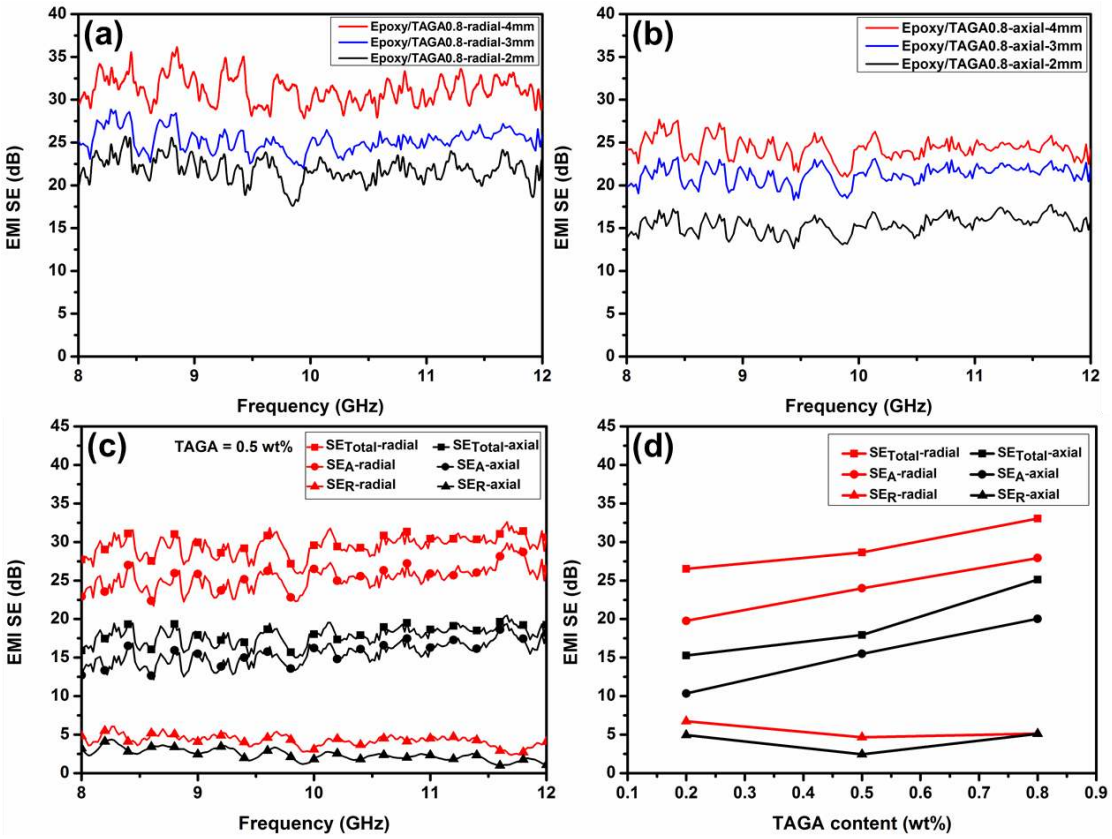

Figure 9. Effect of thickness on EMI SE of the epoxy/TAGA0.8 composite in (a) radical and (b) in axial directions. (c) EMI SE components of the epoxy/TAGA0.5 composite along radial and axial directions. (d) Effect of TAGA content on EMI SE components of epoxy/TAGA composites at the frequency of 9 GHz.

The influences of TAGA content on SE_{Total}, SE_A and SE_R along the two directions are shown in Fig. 9d. With increasing the TAGA contents, SE_A along the two directions increases gradually while SE_R shows a decline tendency. As a given TAGA content, SE_{Total} is mainly contributed by SE_A, due to the absorption-dominated EMI shielding mechanism. The high EMI SE is ascribed to the aligned conducting network that provides abundant interfaces to attenuate the incident waves by multiply reflection inside the composite. Additionally, the higher electrical conductivity along the axial direction also benefits the enhancement in attenuation of the incident waves from the radial direction.

3.4 Anisotropic dynamic mechanical properties of the epoxy composites

The anisotropic dynamic mechanical properties of the epoxy composites are shown in Figure 10. The storage modulus at room temperature varies in the order of epoxy/TAGA0.8 (radial) > epoxy/TGA0.8 > epoxy/TAGA0.8 (axial) > epoxy (Fig. 10a). Because of the highly aligned structure of TAGA, the storage modulus of epoxy/TAGA0.8 composite with only 0.8 wt% TAGA significantly increases to 1.54 GPa along the radial direction, 67.4% and 18.4% larger than that of neat epoxy (0.92 GPa) and epoxy/TGA0.8 composite (1.30 GPa). The glass transition temperature also varies in the same order of epoxy/TAGA0.8 (radial) > epoxy/TGA0.8 > epoxy/TAGA0.8 (axial) > epoxy (Fig. 10b). Higher glass transition temperature indicates stronger interface interaction between graphene and epoxy matrix, resulting in higher modulus of composites.[10,13] The storage modulus (1.21 GPa) and glass transition temperature of the epoxy/TAGA0.8 composite (axial) are smaller than those of epoxy/TGA0.8 composite, which can be ascribed to the splitting of the graphene and epoxy during the measurement.

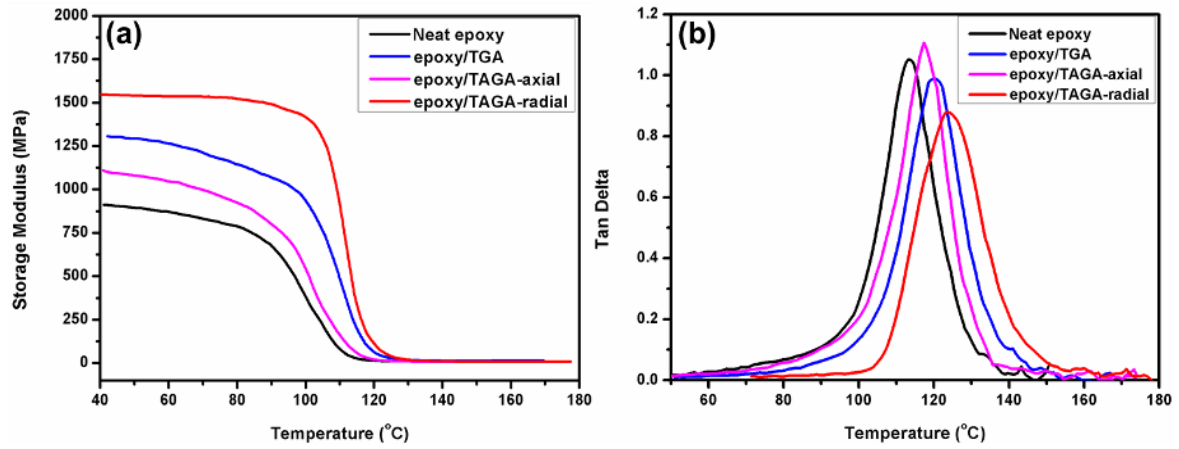

Figure 10. Plots of (a) storage modulus and (b) dynamic loss as a function of temperature for neat epoxy, and epoxy/TGA0.8 and epoxy/TAGA0.8 composites.

4. Conclusion

Highly anisotropic AGAs are facilely prepared by directional-freezing of graphene hydrogels and subsequent freeze-drying, and their anisotropic structure is well preserved during the thermal annealing and subsequent impregnation of epoxy. The fabricated epoxy composites exhibit distinct mechanical, electrical and EMI shielding properties along the axial and radial directions. Due to the alignment of graphene sheets, the numerous polymer/graphene and graphene/graphene interfaces along the radial direction benefit the EMI shielding efficiency of the composites by significantly enhanced multi-reflection and attenuation of the incident electromagnetic waves. The epoxy/TAGA0.8 composite exhibits a high EMI SE of 32 dB along the radial direction and 25 dB along the axial direction. Even with 0.2 wt% of TAGA, the composite presents a high EMI SE of 25 dB along the radical direction, implying that more than 99% of EM waves are shielded. This work shed light on the practical application of AGAs and TAGAs for composites with anisotropic mechanical, electrical and EMI shielding performances.

Acknowledgements

Financial support from the National Key Research and Development Program of China (2016YFC0801302), the National Natural Science Foundation of China (51403016, 51533001, 51521062) and the Fundamental Research Funds for the Central Universities (YS201402) is gratefully acknowledged.

References

(1) Wang, W.; Gumfekar, S. P.; Jiao, Q. J.; Zhao, B. Ferrite-Grafted Polyaniline Nanofibers as Electromagnetic Shielding Materials. *J. Mater. Chem. C* **2013,** 1, 2851-2859.

(2) Liu, W.; Li, H.; Zeng, Q.; Duan, H.; Guo, Y.; Liu, X.; Sun, C.; Liu, H. Fabrication of Ultralight Three-Dimensional Graphene Networks with Strong Electromagnetic Wave Absorption Properties. *J. Mater. Chem. A* **2015,** 3, 3739-3747.

(3) Chung, D. D. L. Carbon Materials for Structural Self-Sensing, Electromagnetic Shielding and Thermal Interfacing. *Carbon* **2012,** 50, 3342-3353.

(4) Sachdev, V. K.; Patel, K.; Bhattacharya, S.; Tandon, R. P. Electromagnetic Interference Shielding of Graphite/Acrylonitrile Butadiene Styrene Composites. *J. Appl. Polym. Sci.* **2011,** 120, 1100-1105.

(5) Rahaman, M.; Chaki, T. K.; Khastgir, D. Development of High Performance EMI Shielding Material from EVA, NBR, and Their Blends: Effect of Carbon Black Structure. *J. Mater. Sci.* **2011,** 46, 3989-3999.

(6) Novoselov, K. S.; Geim, A. K.; Morozov, S. V.; Jiang, D.; Zhang, Y.; Dubonos, S. V.; Grigorieva, I. V.; Firsov, A. A. Electric Field Effect in Atomically Thin Carbon Films. *Science* **2004,** 306, 666-669.

(7) Stoller, M. D.; Park, S.; Zhu, Y.; An, J.; Ruoff, R. S. Graphene-Based Ultracapacitors. *Nano Lett.* **2008,** 8, 3498-3502.

(8) Lee, C.; Wei, X.; Kysar, J. W.; Hone, J. Measurement of the Elastic Properties and Intrinsic Strength of Monolayer Graphene. *Science* **2008,** 321, 385-388.

(9) Balandin, A. A.; Ghosh, S.; Bao, W.; Calizo, I.; Teweldebrhan, D.; Miao, F.; Lau, C. N. Superior Thermal Conductivity of Single-Layer Graphene. *Nano Lett.* **2008,** 8, 902-907.

(10) Tang, G.; Jiang, Z. G.; Li, X.; Zhang, H. B.; Dasari, A.; Yu, Z. Z. Three Dimensional Graphene Aerogels and Their Electrically Conductive Composites. *Carbon* **2014,** 77, 592-599.

(11) Shen, B.; Zhai, W.; Zheng, W. Ultrathin Flexible Graphene Film: An Excellent Thermal Conducting Material with Efficient Emi Shielding. *Adv. Funct. Mater.* **2014,** 24, 4542-4548.

(12) Chen, Y.; Zhang, H. B.; Huang, Y.; Jiang, Y.; Zheng, W. G.; Yu, Z. Z. Magnetic and Electrically Conductive Epoxy/Graphene/Carbonyl Iron Nanocomposites for Efficient Electromagnetic Interference Shielding. *Compos. Sci. Technol.* **2015,** 118, 178-185.

(13) Zeng, Z.; Jin, H.; Chen, M.; Li, W.; Zhou, L.; Zhang, Z. Lightweight and Anisotropic Porous MWCNT/WPU Composites for Ultrahigh Performance Electromagnetic Interference Shielding. *Adv. Funct. Mater.* **2016**, 26, 303-310.

(14) Yan, D. X.; Ren, P. G.; Pang, H.; Fu, Q.; Yang, M. B.; Li, Z. M. Efficient Electromagnetic Interference Shielding of Lightweight Graphene/Polystyrene Composite. *J. Mater. Chem.* **2012,** 22, 18772.

(15) Yan, D. X.; Pang, H.; Li, B.; Vajtai, R.; Xu, L.; Ren, P. G.; Wang, J. H.; Li, Z. M. Structured Reduced Graphene Oxide/Polymer Composites for Ultra-Efficient Electromagnetic Interference Shielding. *Adv. Funct. Mater.* **2015,** 25, 559-566.

(16) Worsley, M. A.; Pauzauskie, P. J.; Olson, T. Y.; Biener, J.; Satcher Jr, J. H.; Baumann, T. F. Synthesis of Graphene Aerogel with High Electrical Conductivity. *J. Am. Chem. Soc.* **2010,** 132, 14067-14069.

(17) Li, C.; Shi, G. Three-Dimensional Graphene Architectures. *Nanoscale* **2012,** *4*, 5549-63.

(18) Chen, Z.; Xu, C.; Ma, C.; Ren, W.; Cheng, H. M. Lightweight and Flexible Graphene Foam Composites for High-Performance Electromagnetic Interference Shielding. *Adv. Mater.* **2013,** 25, 1296-1300.

(19) Yang, Y.; Gupta, M. C.; Dudley, K. L.; Lawrence, R. W. Novel Carbon Nanotube-Polystyrene Foam Composites for Electromagnetic Interference Shielding. *Nano Lett.* **2005,** 5, 2131-2134.

(20) Chung, D. D. L. Electromagnetic Interference Shielding Effectiveness of Carbon Materials. *Carbon* **2001,** 39, 279-285.

(21) Zhang, H. B.; Yan, Q.; Zheng, W. G.; He, Z.; Yu, Z. Z. Tough Graphene-Polymer Microcellular Foams for Electromagnetic Interference Shielding. *ACS Appl. Mater. Interfaces* **2011,** 3, 918-924.

(22) Li, N.; Huang, Y.; Du, F.; He, X.; Lin, X.; Gao, H.; Ma, Y.; Li, F.; Chen, Y.; Eklund, P. C. Electromagnetic Interference (EMI) Shielding of Single-Walled Carbon Nanotube Epoxy Composites. *Nano Lett.* **2006,** 6, 1141-1145.

(23) Xu, Y.; Sheng, K.; Li, C.; Shi, G. Self-Assembled Graphene Hydrogel Via a One-Step Hydrothermal Process. *ACS nano* **2010,** 4, 4324-4330.

(24) Chen, W.; Li, S.; Chen, C.; Yan, L. Self-Assembly and Embedding of Nanoparticles by in Situ Reduced Graphene for Preparation of a 3D Graphene/Nanoparticle Aerogel. *Adv. Mater.* **2011,** 23, 5679-5683.

(25) Chen, W.; Yan, L. In Situ Self-Assembly of Mild Chemical Reduction Graphene for Three-Dimensional Architectures. *Nanoscale* **2011,** 3, 3132-3137.

(26) Wu, Z. S.; Yang, S.; Sun, Y.; Parvez, K.; Feng, X.; Mullen, K. 3D Nitrogen-Doped Graphene Aerogel-Supported Fe_3O_4 Nanoparticles as Efficient Electrocatalysts for the Oxygen Reduction Reaction. *J. Am. Chem. Soc.* **2012,** 134, 9082-9085.

(27) Hu, H.; Zhao, Z.; Wan, W.; Gogotsi, Y.; Qiu, J. Ultralight and Highly Compressible Graphene Aerogels. *Adv. Mater.* **2013,** 25, 2219-2223.

(28) Zhao, Y.; Liu, J.; Hu, Y.; Cheng, H.; Hu, C.; Jiang, C.; Jiang, L.; Cao, A.; Qu, L. Highly Compression-Tolerant Supercapacitor Based on Polypyrrole-Mediated Graphene Foam Electrodes. *Adv. Mater.* **2013,** 25, 591-595.

(29) Yang, L.; Wang, Z.; Ji, Y.; Wang, J.; Xue, G. Highly Ordered 3D Graphene-Based Polymer Composite Materials Fabricated by “Particle-Constructing” Method and Their Outstanding Conductivity. *Macromolecules* **2014,** 47, 1749-1756.

(30) Zhang, R.; Cao, Y.; Li, P.; Zang, X.; Sun, P.; Wang, K.; Zhong, M.; Wei, J.; Wu, D.; Kang, F.; Zhu, H. Three-Dimensional Porous Graphene Sponges Assembled with the Combination of Surfactant and Freeze-Drying. *Nano Res.* **2014,** 7, 1477-1487.

(31) Chen, Z.; Ren, W.; Gao, L.; Liu, B.; Pei, S.; Cheng, H. M. Three-Dimensional Flexible and Conductive Interconnected Graphene Networks Grown by Chemical Vapour Deposition. *Nat. Mater.* **2011,** 10, 424-428.

(32) Liang, J.; Wang, Y.; Huang, Y.; Ma, Y.; Liu, Z.; Cai, J.; Zhang, C.; Gao, H.; Chen, Y. Electromagnetic Interference Shielding of Graphene/Epoxy Composites. *Carbon* **2009,** 47, 922-925.

(33) Liu, T.; Huang, M.; Li, X.; Wang, C.; Gui, C. X.; Yu, Z. Z. Highly Compressible Anisotropic Graphene Aerogels Fabricated by Directional Freezing for Efficient Absorption of Organic Liquids. *Carbon* **2016,** 100, 456-464.

(34) Yousefi, N.; Sun, X.; Lin, X.; Shen, X.; Jia, J.; Zhang, B.; Tang, B.; Chan, M.; Kim, J. K. Highly Aligned Graphene/Polymer Nanocomposites with Excellent Dielectric Properties for High-Performance Electromagnetic Interference Shielding. *Adv. Mater.* **2014,** 26, 5480-5487.

(35) Zhang, H.; Hussain, I.; Brust, M.; Butler, M. F.; Rannard, S. P.; Cooper, A. I. Aligned Two-and Three-Dimensional Structures by Directional Freezing of Polymers and Nanoparticles. *Nat. Mater.* **2005,** 4, 787-793.

(36) Xin, G.; Sun, H.; Scott, S. M.; Yao, T.; Lu, F.; Shao, D.; Hu, T.; Wang, G.; Ran, G.; Lian, J. Advanced Phase Change Composite by Thermally Annealed Defect-Free Graphene for Thermal Energy Storage. *ACS Appl. Mater. Interfaces* **2014,** 6, 15262-15271.

(37) Hummers Jr, W. S.; Offeman, R. E. Preparation of Graphitic Oxide. *J. Am. Chem. Soc.* **1958,** 80, 1339-1339.

(38) Gao, J.; Liu, F.; Liu, Y.; Ma, N.; Wang, Z.; Zhang, X. Environment-Friendly Method to Produce Graphene That Employs Vitamin C and Amino Acid. *Chem. Mater.* **2010,** 22, 2213-2218.

(39) Qiu, L.; Liu, J. Z.; Chang, S. L.; Wu, Y.; Li, D. Biomimetic Superelastic Graphene-Based Cellular Monoliths. *Nat. Commun.* **2012,** 3, 1241.

(40) Zhang, H.; Cooper, A. I., Aligned Porous Structures by Directional Freezing. *Adv. Mater.* **2007,** 19, 1529-1533.

(41) Wang, J.; Xiang, C.; Liu, Q.; Pan, Y.; Guo, J. Ordered Mesoporous Carbon/Fused Silica Composites. *Adv. Funct. Mater.* **2008,** 18, 2995-3002.

(42) Cao, M. S.; Wang, X. X.; Cao, W. Q.; Yuan, J. Ultrathin Graphene: Electrical Properties and Highly Efficient Electromagnetic Interference Shielding. *J. Mater. Chem. C* **2015,** 3, 6589-6599.

(43) Song, W. L.; Wang, J.; Fan, L. Z.; Li, Y.; Wang, C. Y.; Cao, M. S. Interfacial Engineering of Carbon Nanofiber–Graphene–Carbon Nanofiber Heterojunctions in Flexible Lightweight Electromagnetic Shielding Networks. *ACS Appl. Mater. Interfaces* **2014,** 6, 10516-10523.

(44) Worsley, M. A.; Pham, T. T.; Yan, A.; Shin, S. J.; Lee, J. R.; Bagge Hansen, M.; Mickelson, W.; Zettl, A. Synthesis and Characterization of Highly Crystalline Graphene Aerogels. *ACS nano* **2014,** 8, 11013-11022.

(45) Wang, Z.; Shen, X.; Akbari Garakani, M.; Lin, X.; Wu, Y.; Liu, X.; Sun, X.; Kim, J. K. Graphene Aerogel/Epoxy Composites with Exceptional Anisotropic Structure and Properties. *ACS Appl. Mater. Interfaces* **2015,** 7, 5538-5549.

(46) Zeng, X.; Yao, Y.; Gong, Z.; Wang, F.; Sun, R.; Xu, J.; Wong, C. P. Ice-Templated Assembly Strategy to Construct 3D Boron Nitride Nanosheet Networks in Polymer Composites for Thermal Conductivity Improvement. *Small* **2015,** 11, 6205-6213.

(47) Shen, B.; Zhai, W.; Tao, M.; Ling, J.; Zheng, W. Lightweight, Multifunctional Polyetherimide/Graphene@Fe_3O_4 Composite Foams for Shielding of Electromagnetic Pollution. *ACS Appl. Mater. Interfaces* **2013,** 5, 11383-11391.

(48) Yang, Y.; Gupta, M. C.; Dudley, K. L.; Lawrence, R. W. Conductive Carbon Nanofiber–Polymer Foam Structures. *Adv. Mater.* **2005,** 17, 1999-2003.

(49) Jin, M.; Kim, T. H.; Lim, S. C.; Duong, D. L.; Shin, H. J.; Jo, Y. W.; Jeong, H. K.; Chang, J.; Xie, S.; Lee, Y. H. Facile Physical Route to Highly Crystalline Graphene. *Adv. Funct. Mater.* **2011,** 21, 3496-3501.

(50) Chen, Y.; Wang, Y.; Zhang, H. B.; Li, X.; Gui, C. X.; Yu, Z. Z. Enhanced Electromagnetic Interference Shielding Efficiency of Polystyrene/Graphene Composites with Magnetic Fe_3O_4 Nanoparticles. *Carbon* **2015,** 82, 67-76.

(51) Al Saleh, M. H.; Sundararaj, U. Electromagnetic Interference Shielding Mechanisms of CNT/Polymer Composites. *Carbon* **2009,** 47, 1738-1746.

Table of Content Graphic

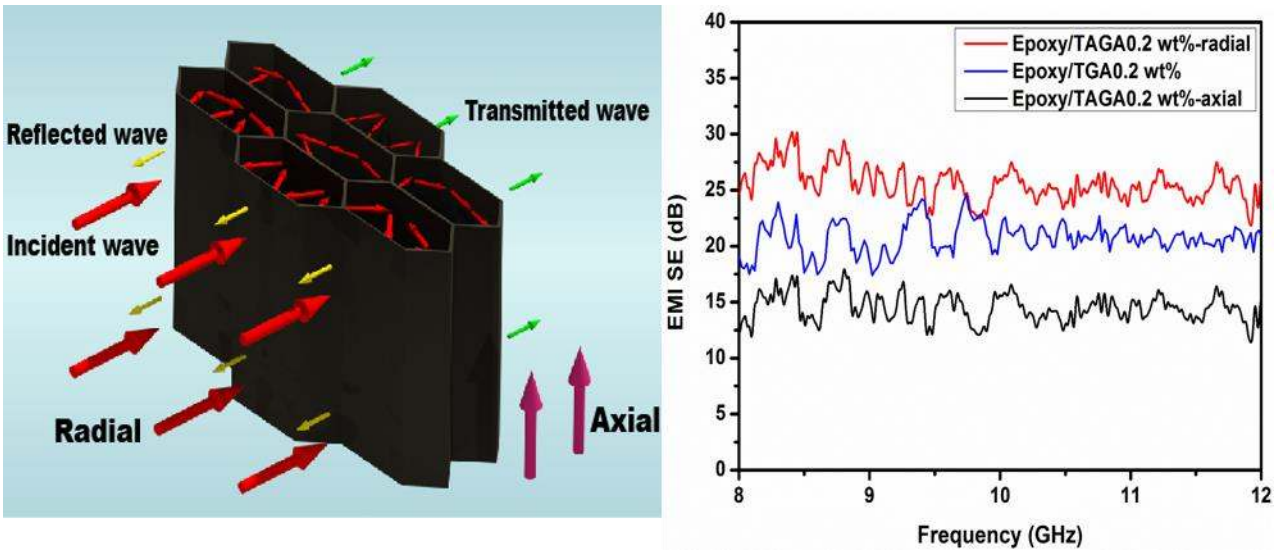

Supporting Information

Thermally Annealed Anisotropic Graphene Aerogels and their Electrically Conductive Epoxy Composites with Excellent Electromagnetic Interference Shielding Efficiencies

Xing-Hua Li[a], *Xiaofeng Li*[a*], *Kai-Ning Liao*[a], *Peng Min*[a], *Tao Liu*[a], *Aravind Dasari*[b] *and Zhong-Zhen Yu*[a,c*]

[a] State Key Laboratory of Organic-Inorganic Composites, College of Materials Science and Engineering, Beijing University of Chemical Technology, Beijing 100029, China

[b] School of Materials Science & Engineering (Blk N4.1), Nanyang Technological University, 50 Nanyang Avenue, Singapore 639798

[c] Beijing Advanced Innovation Center for Soft Matter Science and Engineering, Beijing University of Chemical Technology, Beijing 100029, China

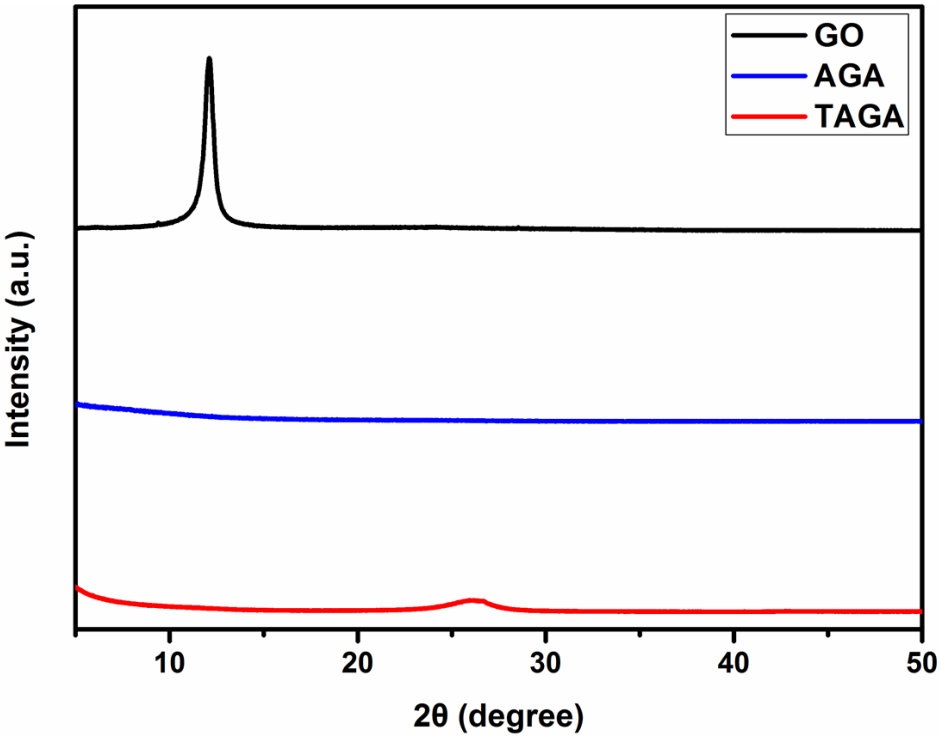

Figure S1. XRD patterns of GO, AGA and TAGA.

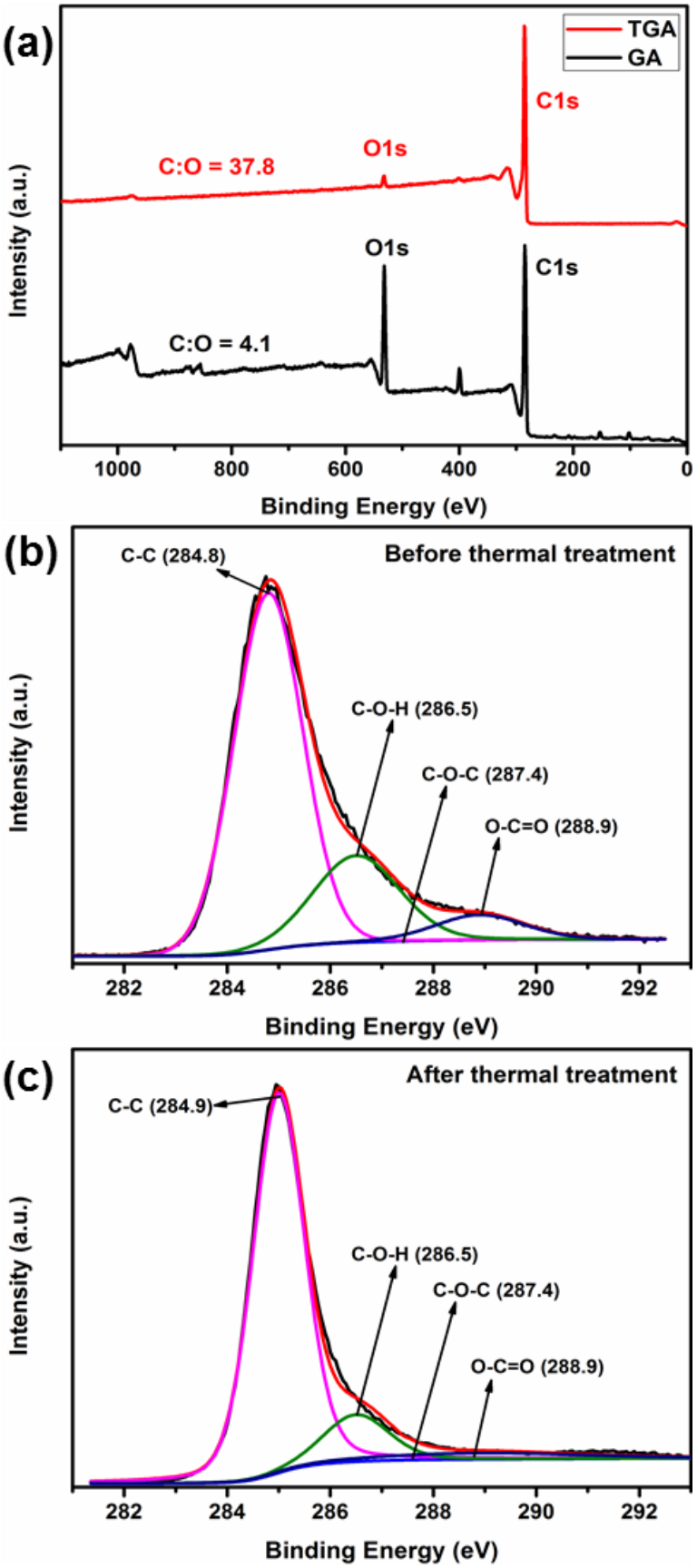

Figure S2. XPS spectra of (a) GA and TGA; XPS C1s curves of (b) GA and (c) TGA.

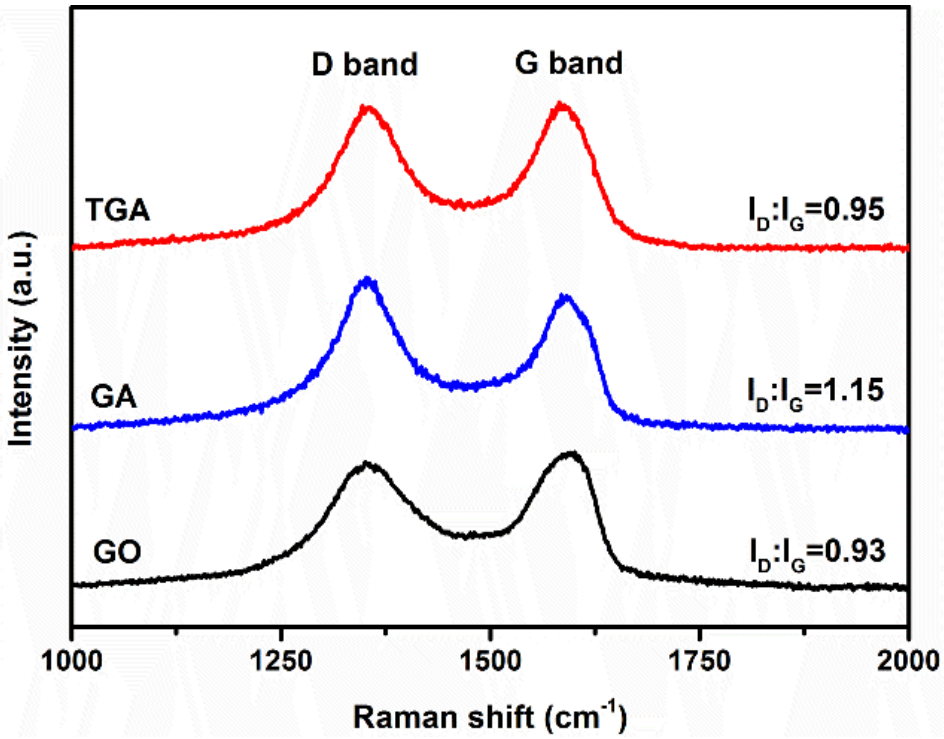

Figure S3. Raman spectra of GO, GA and TGA.

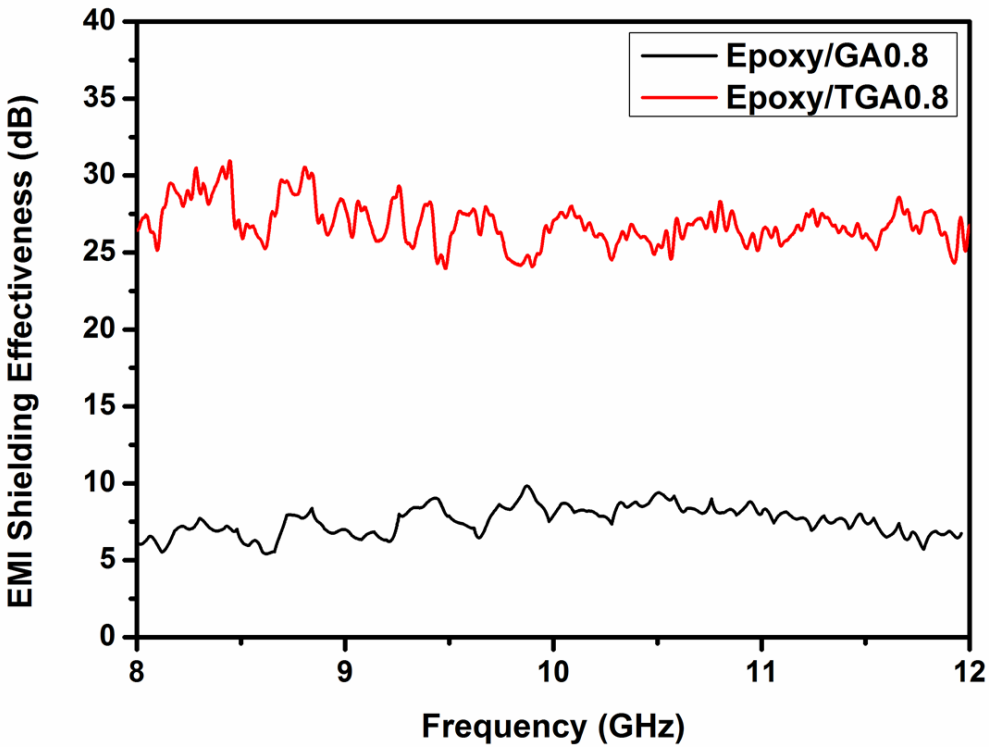

Figure S4. Plots of EMI SE versus frequency for epoxy/GA0.8 and epoxy/TGA0.8 composites.

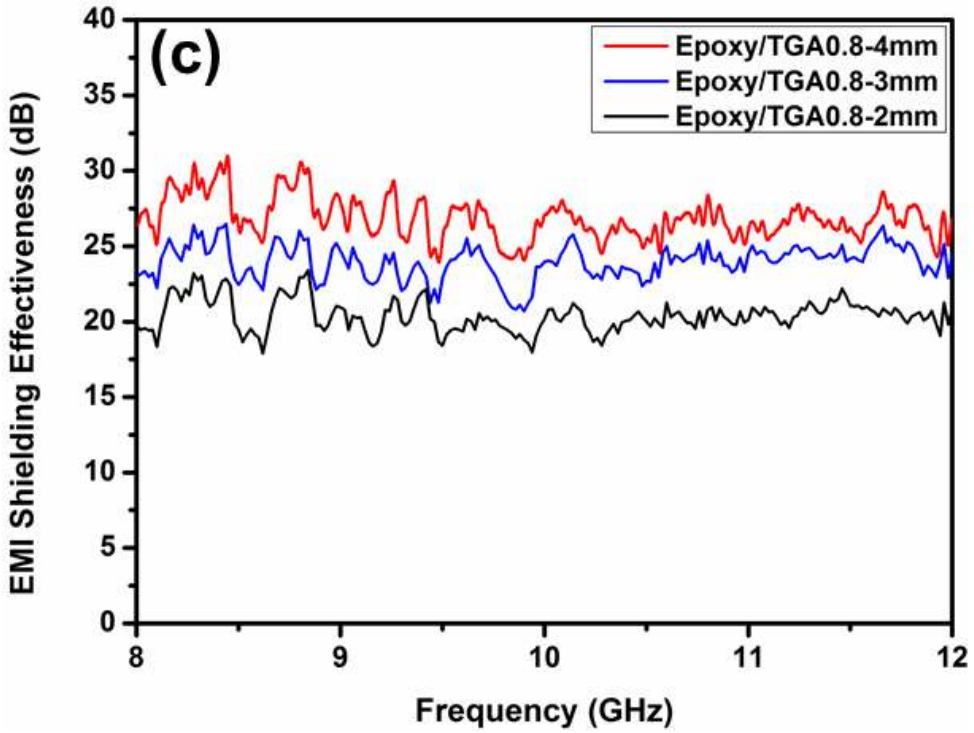

Figure S5. Plots of EMI SE versus frequency for epoxy/TGA0.8 composites with different thicknesses.

Table S1. Comparison of EMI shielding performances of epoxy/TAGA composites with the literature.

Composites[a)]	Content	Thickness (mm)	EMI SE (dB)	Frequency (GHz)	Ref.
PS/Graphene	30 wt%	2.5	29	8.2-12.4	[14]
PS/CNF Foam	15 wt%		≈19	8.2-12.4	[48]
PS/MWNT Foam	7 wt%		20	8.2-12.4	[19]
PEI/Graphene/Fe_3O_4 Foam	10 wt% graphene@Fe_3O_4	2.5	16	8-12	[47]
Epoxy/RGO	15 wt%		21	8.2-12.4	[32]
Epoxy/Aligned RGO	2 wt%	＞0.1	38	0.4-4	[34]
PMMA/Graphene Foam	5 wt%	2.4	19	8-12	[21]
PDMS/Graphene (CVD) Foam	0.8 wt%	≈1	≈30	0.03-1.5	[18]
		≈1	≈22	8-12	
		3~4	≈34	8-12	
WPU/MWNT (Radial)	7.2 vol%	2.3	50.5	8.2-12.4	[13]
Epoxy/TGA	0.8 wt%	4	27	8-12	This work
Epoxy/TAGA (Axial)	0.8 wt%	4	25	8-12	This work
Epoxy/TAGA (Radial)	0.8 wt%	4	32	8-12	This work
Epoxy/TAGA (Radial)	0.2 wt%	4	25	8-12	This work

[a)] PS-polystyrene; PMMA-polymethylmethacrylate; PDMS-polydimethylsiloxane; WPU-water-borne polyurethane; PEI-polyetherimide